

# Rationally Designed Dual-Mode Triboelectric Nanogenerator for Harvesting Mechanical Energy by Both Electrostatic Induction and Dielectric Breakdown Effects

Linglin Zhou, Di Liu, Shaoxin Li, Zhihao Zhao, Chunlei Zhang, Xin Yin, Li Liu, Shengnan Cui, Zhong Lin Wang,\* and Jie Wang\*

With the advantages of its light weight, low cost, and high efficiency especially at low operation frequency, the triboelectric nanogenerator (TENG) is considered to be a potential solution for self-powered sensor networks and large-scale renewable blue energy. However, the conventional TENG converts mechanical energy into electrical energy only via either electrostatic induction or electrostatic breakdown. Here, a novel dual-mode TENG is presented, which can simultaneously harvest mechanical energy by electrostatic induction and dielectric breakdown in a single device. Based on the complementary working mechanism, it achieves a great improvement in the output performance with the sum of two TENGs via a single mechanism and reveals the effect of dielectric layer thickness on the triboelectrification, electrostatic induction, and air breakdown. This study establishes a new methodology to optimize TENGs and provides a new tool to investigate the triboelectrification, electrostatic induction and dielectric breakdown simultaneously.

environment as the energy of a new era.<sup>[1–4]</sup> Among various kinds of distributed energy, ambient mechanical energy provides a promising power source because of its wide distribution and sufficient availability. With desirable merits of simple structure, light weight, broad material availability, low cost, and high efficiency even at low-frequency operation, the triboelectric nanogenerators (TENGs) have been proved as an alternative technology for extracting ambient mechanical energy that is ubiquitous and almost endless.<sup>[5–8]</sup> Based on the coupling effect of triboelectrification and electrostatic induction, the conventional TENG, called AC-TENG here due to its alternating current (AC) output character, can convert mechanical energy into electrical energy, which have exhibited great potential to operate as self-charging

## 1. Introduction

As the world marches into the era of internet of things (IoT), robotics and artificial, large efforts have been devoted to developing sustainable, clean, mobile, and distributed energy from

power system<sup>[9–14]</sup> and self-powered sensors.<sup>[15–19]</sup> As an energy generator, the extensive application of TENG highly depends on its output power density and energy conversion efficiency, which are dictated by the triboelectric charge density quadratically. Recently, a great deal of research has been focused on materials selection,<sup>[20,21]</sup> surface modification,<sup>[22]</sup> environment optimization,<sup>[23–25]</sup> structure design,<sup>[26–28]</sup> and ultrathin dielectric layer utilization<sup>[29,30]</sup> to enhance the triboelectric charges. Nevertheless, the electrostatic breakdown effect in ambient environment can inevitably reduce the triboelectric charges, causing the loss of the electrostatic energy.<sup>[31]</sup> On the other hand, the maximal surface charge density can be achieved after several cycles through charge accumulation process.<sup>[32]</sup> Therefore, the following triboelectrification process is invalid for charge accumulation, which will further reduce the energy conversion efficiency.

Currently, direct current triboelectric nanogenerators (DC-TENGs), based on the conjunction of triboelectrification and electrostatic breakdown, have been developed for directly converting mechanical energy to a constant current.<sup>[33–35]</sup> Compared to traditional TENGs obtain a DC output based on electrostatic induction by using a full-wave rectifier, rotary rectifier bridge,<sup>[36]</sup> or a multi-phase rotation-type structure,<sup>[37]</sup> DC-TENG can supply a constant current power source to directly power electronics without any rectifier or energy storage devices, which can serve as a promising solution to miniaturize the self-powered systems for the era of distributed electronic devices.

Dr. L. Zhou, D. Liu, S. Li, Dr. Z. Zhao, C. Zhang, X. Yin, L. Liu, S. Cui, Prof. Z. L. Wang, Prof. J. Wang  
Beijing Institute of Nanoenergy and Nanosystems  
Chinese Academy of Sciences  
Beijing 100083, China  
E-mail: zhong.wang@mse.gatech.edu; wangjie@binn.cas.cn

Dr. L. Zhou, D. Liu, S. Li, C. Zhang, X. Yin, L. Liu, S. Cui, Prof. Z. L. Wang, Prof. J. Wang  
College of Nanoscience and Technology  
University of Chinese Academy of Sciences  
Beijing 100049, P. R. China

Dr. Z. Zhao  
School of Materials  
Sun Yat-sen University  
Guangzhou 510275, P. R. China

Prof. Z. L. Wang  
School of Materials Science and Engineering  
Georgia Institute of Technology  
Atlanta, GA 30332, USA

 The ORCID identification number(s) for the author(s) of this article can be found under <https://doi.org/10.1002/aenm.202000965>.

DOI: 10.1002/aenm.202000965

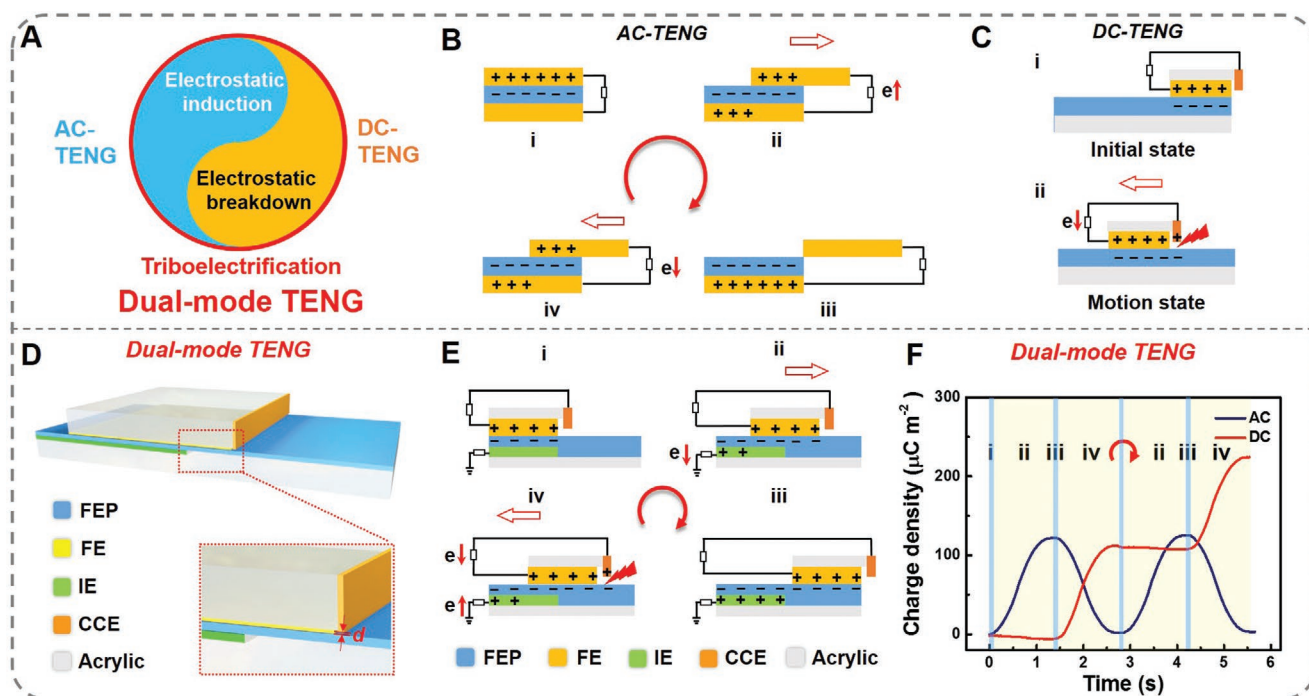


**Figure 1.** The development of TENG for harvesting mechanical energy based on triboelectrification, electrostatic induction, and electrostatic breakdown. A) Different mode TENGs for harvesting mechanical energy based on triboelectrification, electrostatic induction, and electrostatic breakdown. B) Working mechanism of conventional AC-TENG. C) Working mechanism of DC-TENG. D) A schematic illustration of sliding dual-mode TENG proposed in this work. E) Working mechanism of dual-mode TENG in a full cyclic motion. F) Surface charge density of the dual-mode TENG.

However, only parts of triboelectric charges can be collected by DC-TENG via breakdown effect, where the other parts still remain on the surface of dielectric film. Based on triboelectrification, the generated electrostatic charges can be transferred to electricity energy by electrostatic induction and electrostatic breakdown. Therefore, the charge values of AC-TENG via electrostatic induction and DC-TENG via electrostatic breakdown can approximately be regarded as a complementary set that mainly consists of the total triboelectric charge quantity as shown in **Figure 1A**. However, previous works can extract mechanical energy after triboelectrification process only by one of the mentioned two technologies, that either AC-TENG or DC-TENG, where another part of the triboelectric charges is always difficult to harvest. Therefore, harvesting the total triboelectric charge quantity to enhance the performance of TENGs is highly desired.

In this work, we develop a dual-mode TENG for harvesting mechanical energy by the conjunction of triboelectrification, electrostatic induction, and electrostatic breakdown effects. Based on the working principle, both AC and DC can be simultaneously generated in a device, where the total output is a sum of a single AC-TENG and a single DC-TENG with the same structure. The improvement of total output performance is demonstrated through both sliding dual-mode TENG and rotary dual-mode TENG. With the independence of AC and DC outputs, the sliding dual-mode TENG is used to investigate the effect of dielectric layer thickness on the output of AC-TENG and DC-TENG at the same time. This work not only provides a new optimized methodology for TENG to enhance its output

performance, but also gives an effective tool to study triboelectrification, electrostatic induction, and electrostatic breakdown.

## 2. Results and Discussion

### 2.1. Principle of Dual-Mode TENG

The conventional TENG converts mechanical energy into electrical energy only via either electrostatic induction or electrostatic breakdown separately. For harvesting the total triboelectric charge quantity to enhance the performance of TENGs, we propose a novel dual-mode TENG to simultaneously harvest mechanical energy by electrostatic induction and dielectric breakdown effects (**Figure 1A**). The dual-mode TENG is built on the integration of conventional AC-TENG and DC-TENG, where it can adopt either sliding mode or rotary mode to harvest the total triboelectric charge quantity.

Previous works have been demonstrated the sliding-mode AC-TENG,<sup>[38,39]</sup> where a typical AC output will be achieved based on the working principle of triboelectrification effect and electrostatic induction (**Figure 1B**; **Figure S1** and **Note S1**, Supporting Information). In this mode, the electrode and dielectric layer move with each other in the horizontal direction, where only half of the space can be utilized to generate triboelectric charges. As for the DC-TENG,<sup>[35]</sup> based on the triboelectrification effect and electrostatic breakdown, a constant current can be achieved by simply sliding on a triboelectric film (**Figure 1C**; **Figure S1** and **Note S2**, Supporting Information).

Here, we present a dual-mode TENG that can simultaneously harvest mechanical energy by the coupling effects of triboelectrification, electrostatic induction, and electrostatic breakdown in a single device. The structural scheme of the dual-mode TENG is illustrated in Figure 1D. It mainly consists of a stator and a slider working in the sliding mode. Specifically, the stator contains an induction electrode (IE) connected to dielectric film as triboelectric layer; here, fluorinated ethylene propylene (FEP) is used. The slider is similar to that of DC-TENG, which is mainly composed a frictional electrode (FE) and a charge collecting electrode (CCE) with a minute gap to triboelectric layer. The FE and IE set to the same size, both of which are only half the size of FEP film. The detailed fabrication process is described in the Experimental Section.

The working mechanism of dual-mode TENG is shown in Figure 1E. If physical contact occurs between the two surfaces of FEP film and FE layer that display a distinct surface electron affinity, there are negative charges on the FEP film and positive charges on the FE layer due to triboelectrification effect (Figure 1E[i]). Driving by applied force in the direction parallel to the interface, a relative displacement will be formed. With the change of the contact surface area, a potential difference across IE and the FE will be produced, resulting in a current signal in external circuit to balance the potential difference (Figure 1E[ii]). During this process, a continuous signal will be obtained until the FE completely separated from the top of IE (Figure 1E[iii]). Once the slider moves backward, the electrons will flow back and an opposite current will be realized, finally producing a pulse AC signal in one cycle of operation. Meanwhile, owing to the electret effect, FEP film can hold a quasi-permanent electric charge. Therefore, in the backward motion, a very high electrostatic field will be built between the FEP film and CCE. If the electrostatic field is high enough to ionize the air dielectric, where the value is approximately  $3 \text{ kV mm}^{-1}$  from Paschen' Law, air breakdown will occur between the FEP film and CCE, leading to electrons transfer from FEP film to CCE to reduce the potential difference, and finally to FE through external circuit (Figure 1E[iv]). The discharge process will continue during the backward motion process, resulting in a single direction of electrons flow. Therefore, AC and DC outputs can be simultaneously generated through periodic operation process (Figure 1F; Movie S1, Supporting Information). The working mechanism of dual-mode TENG is further demonstrated by using three signal output ports (Figure S2 and Note S3, Supporting Information). Besides, the influence of different connection mode on the performance of dual-mode TENG is investigated as presented in Figure S3, Supporting Information. It is found that the values of AC and DC of dual-mode TENG are almost the same with different connection mode, indicating that the output performance of dual-mode is not affected by the connection mode.

Calculated according to the effective sliding area (Figure S4, Supporting Information), the surface charge densities of single sliding mode AC-TENG and single DC-TENG with FEP film with a thickness of  $230 \mu\text{m}$  are  $127$  and  $112 \mu\text{C m}^{-2}$  (Figure S1, Supporting Information), respectively. By using a single device, dual-mode TENG simultaneously harvests both of the AC and DC outputs with almost the same value of two TENGs via single mechanism (Figure 1F), which greatly improves the

total output performance of TENG with a larger space utilization efficiency.

## 2.2. Performance of Sliding Dual-Mode TENG

The photograph of two parts of sliding dual-mode TENG is shown in Figure S5, Supporting Information. To measure the output performance of sliding dual-mode TENG, the device is driven by a programmable liner motor to create the sliding motion. The charge density, current density, and open-circuit voltage ( $V_{OC}$ ) of the sliding dual-mode TENG are displayed in Figure 2. As for the charge density, both of the DC and AC values almost keep a constant ( $\approx 115 \mu\text{C m}^{-2}$  of DC and  $\approx 130 \mu\text{C m}^{-2}$  of AC) at different accelerations (Figure 2A), which is because that the transferred charge highly depends on the collected charge area after triboelectrification. Besides, the current density and  $V_{OC}$  increase with acceleration because it is highly related to the charge transfer rate. With acceleration increasing, the current density of DC increases from  $229 \mu\text{A m}^{-2}$  at  $0.1 \text{ m s}^{-2}$  to  $672 \mu\text{A m}^{-2}$  at  $0.8 \text{ m s}^{-2}$ , while the value of AC improves from  $282$  to  $833 \mu\text{A m}^{-2}$  (Figure 2B). The corresponding  $V_{OC}$  of DC also increases from  $6$  to  $16 \text{ V}$ , while the  $V_{OC}$  of AC keeps a constant value of  $129 \text{ V}$  (Figure 2C). In addition, the current density and  $V_{OC}$  also change with velocities. With the velocities increasing from  $0.01$  to  $0.04 \text{ m s}^{-1}$ , the current density of DC enhances from  $60$  to  $408 \mu\text{A m}^{-2}$ , while the value of AC improves from  $67$  to  $627 \mu\text{A m}^{-2}$  (Figure 2D). Correspondingly, the  $V_{OC}$  of DC also increases with velocity from  $1.5$  to  $10 \text{ V}$ , while the  $V_{OC}$  of AC keeps a stable value of  $138 \text{ V}$  (Figure 2E). Based on the above working mechanism and experimental results, it can be found that the output of dual-mode TENG is the sum value of a single AC-TENG and DC-TENG, which improves the total performance of TENGs. In addition, the output performance of AC and DC in sliding dual-mode TENG is independent. Therefore, the dual-mode TENG not only can highly improve the total output performance of TENGs, but also can be used to symmetrically investigate the effect of various factors on the triboelectrification, electrostatic induction, and electrostatic breakdown effects.

As a key factor, the thickness of dielectric film has a significant impact on the output performance of TENG. Therefore, investigating the effect of dielectric film thickness on the triboelectrification, electrostatic induction, and electrostatic breakdown effect is favorable to guide the design of TENG. By using the proposed dual-mode TENG, the influence of FEP thickness on both of the AC and DC output is investigated as shown in Figure 2F–H. With the thickness of FEP film decreasing from  $230$  to  $30 \mu\text{m}$ , the charge densities of DC during one cycle are almost keep a constant value of  $115 \mu\text{C m}^{-2}$ , which is much higher than those of DC-TENGs based on electrostatic breakdown.<sup>[34]</sup> Furthermore, the charge density of dual-mode TENG can be further improved by introducing nano-structure on the surface of FEP film, reducing the gap distance between FEP and CCE, adding two CCEs at the both ends of slider.<sup>[35]</sup> While the value of AC increases from  $127$  to  $309 \mu\text{C m}^{-2}$ , which is extremely close to the theoretical value with air breakdown.<sup>[40]</sup> Similarly, the current density and  $V_{OC}$  of DC almost keep a constant value of about  $205 \mu\text{A m}^{-2}$  and  $4 \text{ V}$ , while the current

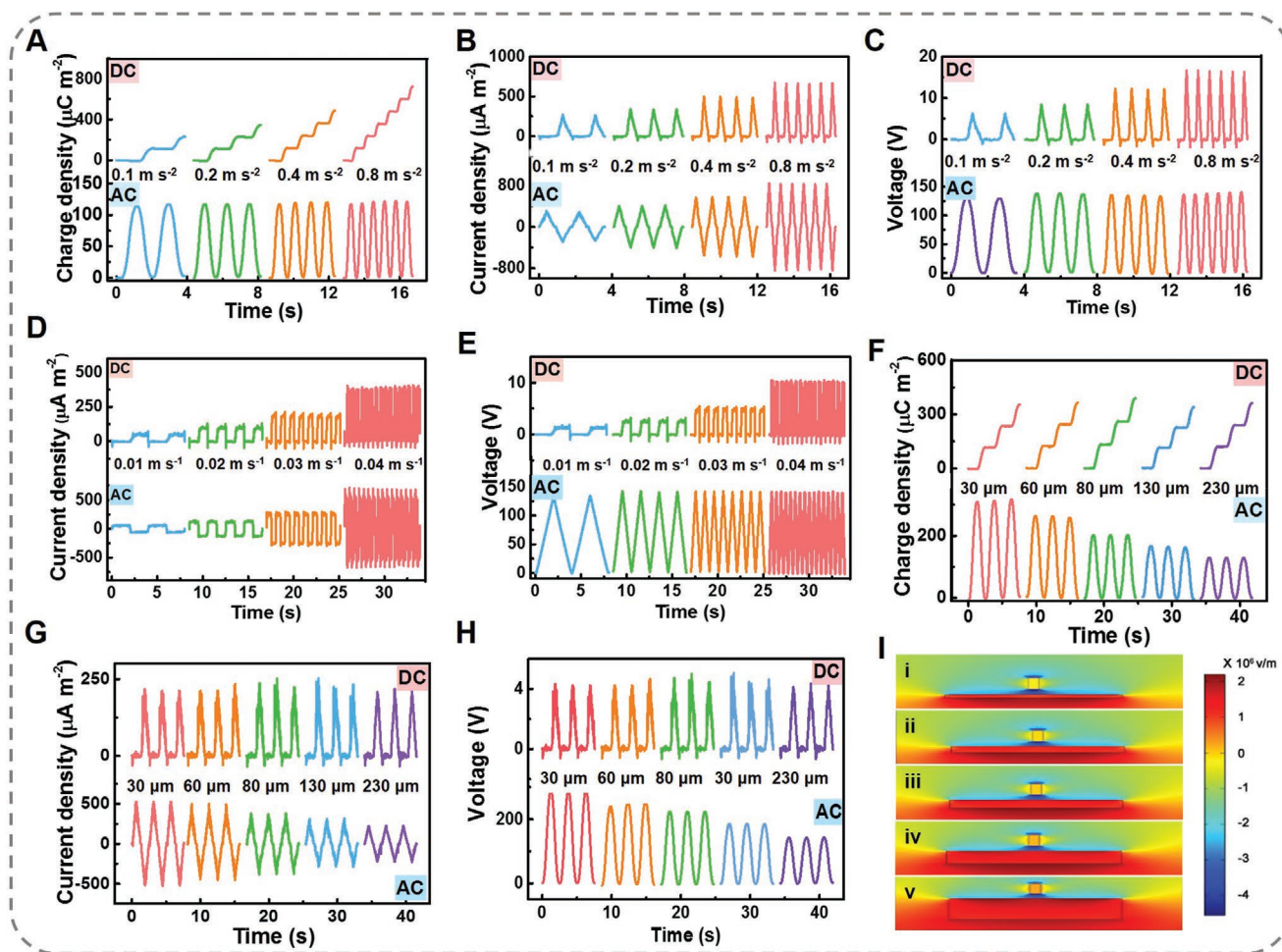


**Figure 2.** Output performance of sliding dual-mode TENG. A) Charge density, B) current density, and C) open-circuit voltage of the sliding dual-mode TENG at different accelerations with 230- $\mu\text{m}$  FEP film. D) Current density and E) open-circuit voltage of the sliding dual-mode TENG at different velocities with 230- $\mu\text{m}$  FEP film. F) Surface charge density, G) current density, and H) open-circuit voltage of the sliding dual-mode TENG at different thickness of FEP film. I) Distribution of the electric field between the CCE and triboelectric layer at different thickness of FEP film.

density and  $V_{OC}$  of AC improve from 218 to 528  $\mu\text{A m}^{-2}$ , and from 142 to 288 V, respectively. Through the finite element analysis method based on COMSOL software, the electrostatic field intensity between the CCE and FEP film is independent of the FEP thickness (Figure 2I), which explains well the stable performance of DC at different thickness of FEP film. The performance of AC improve with the decreasing of FEP thickness might because the inevitable air breakdown in practice, which has been confirmed that the maximum charge density will increase with decreasing the thickness of dielectric film if there is air breakdown phenomena.<sup>[40,41]</sup> These results indicate that better performance of electrostatic induction is attained in a thinner dielectric layer, while the influence of film thickness on electrostatic breakdown is very limited. For this guidance, a high output of AC-TENG can be realized by using an ultrathin dielectric layer, and the stability of DC-TENG without loss of the output can be achieved by using a thicker dielectric film. Moreover, the long-term output current density of sliding dual-mode TENG is investigated as presented in Figure S6, Supporting Information. After working 3000 s, the values of AC

and DC are nearly keep constant, indicating a good stability. As one of the key concerns regarding TENG, especially for sliding mode TENGs, developing materials that have the most robust mechanical durability and stability, and using a conjunction of working modes for TENG are the two possible strategies to solve this issue.<sup>[42]</sup>

### 2.3. Performance of Rotary Dual-Mode TENG

A radial-arrayed rotary dual-mode TENG is achieved via the parallel multiple sliding dual-mode TENGs. With a multilayered structure, the rotary dual-mode TENG mainly composes of a rotator and a stator, as displayed in Figure 3A,B. Both of the rotator and stator consist of radially-arrayed sectors, where each unit is similar to a sliding dual-mode TENG. In this structure, all the CCE and FE are connected in parallel, respectively. Moreover, a foam on the bottom of IE is used as buffer layer to guarantee the effective contact between the FE and triboelectric layer.

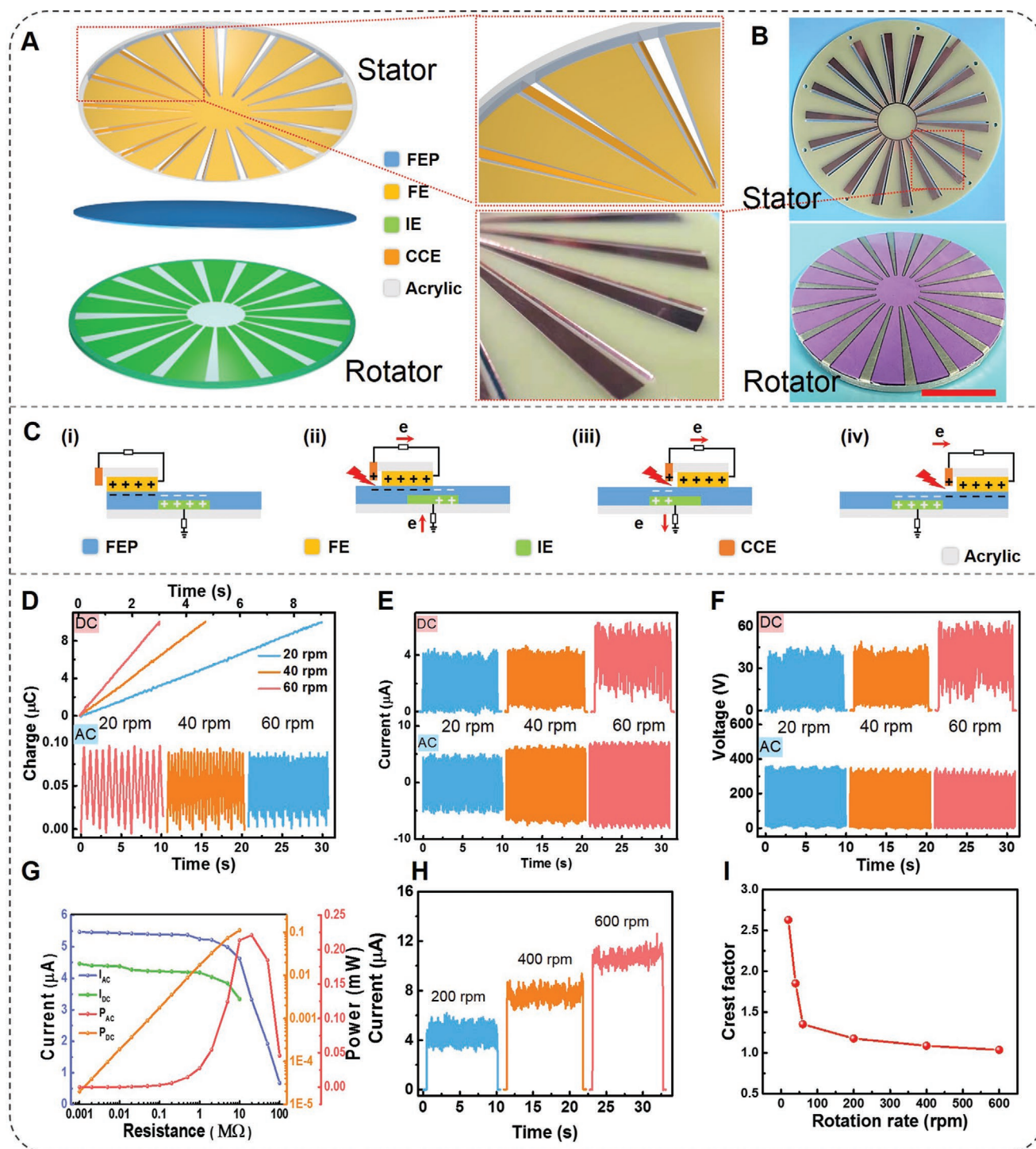


**Figure 3.** The working mechanism and output performance of rotary dual-mode TENG. A) Schematic illustration of rotary dual-mode TENG (inset shows the enlarge illustration of the stator). B) Photographs of the rotary mode TENG (scale bar, 5 cm). C) Working mechanism of rotary dual-mode TENG. D) Transferred charges, E) short-circuit current, and F) open-circuit voltage of rotary dual-mode TENG at different rotation rates. G) Output current and power of rotary dual-mode TENG with various resistances. H) Short-circuit current of rotary dual-mode TENG at high rotation rates. I) Crest factor of rotary dual-mode TENG at different rotation rates.

The operation of rotary dual-mode TENG is based on a relative rotation between the rotator and stator. Different from the sliding mode, the CCE of rotary dual-mode TENG will pass

through the IE during the movement. Therefore, an experiment was conducted to investigate the working principle and output performance of dual-mode TENG when the CE passes through

the IE part. As shown in Figure S7, Supporting Information, when the CCE closes to the IE from state (i) to (ii) (Figure S7A, Supporting Information), the DC and AC are independent of each other as the above sliding mode. In this stage, both of DC and AC are obtained as the mechanism of sliding dual-mode TENG, where the transferred charges of DC and AC are 35 and 48 nC, respectively (the red background part of Figure S7B, Supporting Information). When the CCE go through the IE as the state from (ii) to (iv), a DC with 27 nC and a reversed AC with 32 nC are also harvested (the blue background part of Figure S7B, Supporting Information). It means that both electrostatic induction and electrostatic breakdown take place on the FEP where is upon the IE layer. A similar change can be more obviously reflected from the  $I_{SC}$  of DC and AC in different working states (Figure S7C, Supporting Information). The smaller output of DC in the later process is because that triboelectrification on FEP film is shielded by CCE. Meanwhile, the residual static charges after triboelectrification still are stored on the surface of FEP films, resulting in the AC output based on the triboelectrification in the later process (Figure 3C). The working mechanism of rotary dual-mode TENG at first cycle is elaborated in Figure S8 and Note S4, Supporting Information.

It is noteworthy that when the CCE passes through the IE, the total transferred charges in one cycle can be regarded as the sum value of DC and AC during this process, which can be calculated as 142 nC, and it is higher than the 131 nC obtained in previous dual-mode TENG that the slider moves forth and back. The result indicates that the collection of total triboelectric charges in one cycle can be further improved through the coupling effects of electrostatic induction and electrostatic breakdown. Generally, air breakdown could dissipate the static charges on the surface of dielectric film, thus new triboelectric charges will be generated via the operation of rotary dual-mode TENG in each cycle. Based on this, part of the newly generated triboelectric charges will be extracted to produce DC, and the residual parts can be harvested to generate AC. Besides, owing to the high efficiency to generate triboelectric charges of the sliding and rotary modes, the fabricated dual-mode TENG can not only harvest mechanical energy by breakdown effect that always induces the loss of the electrostatic energy, but also improves the triboelectrification effect that usually is invalid after reaching the saturation surface charge density, which further enhances the collection of total triboelectric charges, and thus improves the energy conversion efficiency of TENG.

As a major factor, the influence of rotation speed on the performance of the rotary dual-mode TENG was also investigated as shown in Figure 3D–F. With the rotation speed ranging from 20 to 60 rpm, the transferred charge speed, short-circuit current ( $I_{SC}$ ), and  $V_{OC}$  of DC part increase from 1.0 to 3.5  $\mu\text{C s}^{-1}$ , from 4.3 to 6.1  $\mu\text{A}$ , and from 43 to 61 V, respectively. In addition, the transferred charge and  $V_{OC}$  of AC part almost keeps a stable value of  $\approx 94$  nC and  $\approx 352$  V, while the corresponding  $I_{SC}$  increases from 4.6 to 6.7  $\mu\text{A}$ , respectively. Once connecting an external load, the current value of DC is almost stable, the corresponding power output improves linearly with the load resistance increasing, from 0.02  $\mu\text{W}$  to 0.11 mW with the load increasing from 0.001 to 10 M $\Omega$  (Figure 3G), which can be further improved with external load increasing. In addition, the current of AC declines with the load resistance increasing, and the maximal output power

reaches 0.22 mW in the matched load of 20 M $\Omega$  at rotation speed of 40 rpm (Figure 3G). If further improving the rotation speed to 600 rpm, the current of DC increases to 11.2  $\mu\text{A}$  (Figure 3H). Interestingly, with the rotation speed increasing, the average peak current of DC part is close to the equivalent current (Figure S9, Supporting Information), and its crest factor approaches to 1 (Figure 3I). From the above results, a constant current output would be realized in a higher rotation speed.

#### 2.4. Application of Dual-Mode TENG to Drive Electronic Devices

To demonstrate the enhanced output performance of the dual-mode TENG, a rotary dual-mode TENG is applied to drive various electronic devices together with an energy storage unit at 60 rpm. The system diagram is depicted in Figure 4A, where the DC part is directly connected with a capacitor of 4.7  $\mu\text{F}$ , while AC part and the capacitor are connected by a full-wave rectifier. The corresponding circuit diagram is displayed Figure 4B. When switch K1, K2, and K3 are on and K4 is off, the dual-mode TENG can be utilized to charge capacitor to 10 V in 4.8 s with the integrated output (Figure 4C), and the equivalent charging current ( $I_c$ ) can be calculated as 9.78  $\mu\text{A}$  (Note S5, Supporting Information). By using a single AC or DC output, the charging rate obviously declines, and the charging currents decrease to 6.5 and 3.6  $\mu\text{A}$ , respectively.

When all the switches are on, the dual-mode TENG can be used to be a self-powered system with a capacitance (220  $\mu\text{F}$ , here) to drive an electronic calculator (Figure 4D). Monitored by a voltmeter, a declined voltage of the capacitor is observed when it powers the calculator alone with the discharging current of 3.2  $\mu\text{A}$ . When the dual-mode TENG works, the voltage increases with an integrated charging current of 4.49  $\mu\text{A}$ , and the calculator is driven simultaneously (Figure 4E). Even though the single DC output or AC output of dual-mode TENG can drive the electronic calculator as well, the charging currents of them are much lower, which are 1.29 and 3.36  $\mu\text{A}$ , respectively (Figure 4F,G).

### 3. Conclusion

In this work, we have proposed a dual-mode TENG to effectively convert mechanical energy into electricity based on the coupling effects of triboelectrification, electrostatic induction, and electrostatic breakdown. According to the complementary working mechanism, triboelectric charges generated in one cycle can be simultaneously harvested by electrostatic induction and electrostatic breakdown effects, which generates AC and DC outputs at the same time in a single device. Comparing with the two TENGs via single mechanism, the total output of dual-mode TENG is largely improved with a high triboelectrification effectiveness, which is demonstrated through both sliding dual-mode TENG and rotary dual-mode TENG. Besides, the sliding dual-mode TENG enable to symmetrically investigate the impact of factors such as dielectric layer thickness on triboelectrification, electrostatic induction, and air breakdown, which can be a guidance to design both AC-TENG and DC-TENG. This study establishes a new methodology to

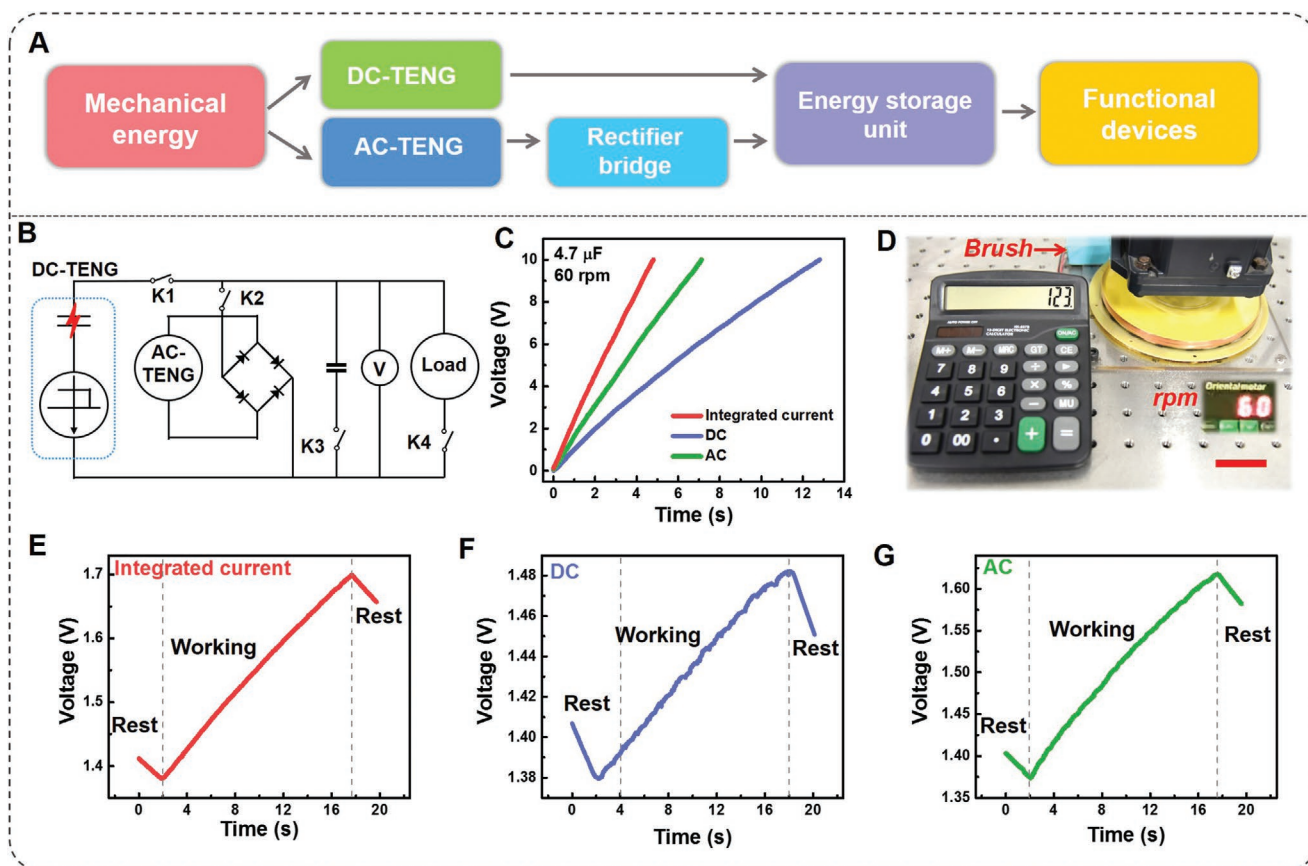


**Figure 4.** Application of the dual-mode TENG to drive electronic devices. A) System diagram and B) circuit diagram of the self-powered system for powering electronics with energy storage units. C) Charging curves of the capacitor ( $4.4 \mu\text{F}$ ) by dual-mode TENG at 60 rpm. D) Photograph of a watch driven by dual-mode TENG (scale bar, 5 cm). Charging curves of the capacitor when the calculator is driven by dual-mode TENG simultaneously with E) integrated output, F) DC output, and G) AC output.

optimize TENG and provides a new tool to investigate the triboelectrification, electrostatic induction, and dielectric breakdown simultaneously.

#### 4. Experimental Section

**Fabrication of the Sliding Dual-Mode TENG:** A commercialized PCB with dimensions  $20 \times 20 \times 1.6$  mm was used as the slider, where a pre-deposited Cu film on the surface of PCB board acted as friction electrode. Between the friction electrode and the left end of the PCB board, there was a tiny distance of about 1 mm. A rectangle Cu foil with dimensions of  $20 \times 1.6 \times 0.05$  mm was pasted on the left side of PCB board as charge collecting electrode, where a tiny gap also was between the charge collecting electrode and triboelectric layer. As for the stator, an acrylic board was cut into a rectangle acrylic sheet with dimensions of  $40 \times 20 \times 5$  mm by using a laser cutter (PLS6.75, Universal Laser Systems), acting as the substrate. A  $40 \times 20 \times 2$  mm foam was adhered on top of the substrate to ensure the contact intimacy. Then, an FEP film with dimensions of  $40 \times 20 \times 2$  mm, deposited with a thin  $20 \times 20$  mm Cu layer by vacuum magnetron sputtering on the bottom and left side as induction electrode, was adhered to the foam as the triboelectric layer.

**Fabrication of the Rotary Dual-Mode TENG:** For the rotor, an acrylic board was cut into a disc-shape with a diameter of 14 cm and a thickness of 3 mm, acting as substrate. A through-hole was drilled at the center of the acrylic sheet to connect the rotational motor. After that, a foam with the same size was adhered on the surface of the substrate

as the buffer layer. Then, a collection of radially arrayed conductive fabric with a central angle of  $10^\circ$  was attached on the surface of foam, all the conductive fabrics were connected on the side of the substrate as the induction electrodes. In the operation, a brush was always used to connect the conductive fabrics for collecting current. Lastly, FEP film with thickness of  $230 \mu\text{m}$  was adhered on the surface of conductive fabric as triboelectric layer. As for the stator, an acrylic board with a central angle of  $2^\circ$ , a diameter of 14 cm, and a thickness of 5 mm was used as the substrate. Then, a PCB board with the same shape and size was stuck on the surface of substrate, where pre-deposited copper film with the same shape and size of conductive fabric was used as frictional electrodes. The frictional electrodes were mutually connected with one another. After that, the Cu foils with dimensions of  $140 \times 2 \times 0.05$  mm were pasted at the right side of the PCB board with a minimum gap between the FEP film and Cu foils.

**COMSOL Simulation:** The 2D potential distribution between two the CCE and charged FEP films was calculated using the commercial software COMSOL. The distance between the CCE and FEP layer was set to be 0.5 mm, and the potential distribution was investigated at different thickness of FEP with 30, 60, 80, 130, and  $230 \mu\text{m}$ , respectively. The surface charge density of each FEP film was  $50 \mu\text{C m}^{-2}$ .

**Measurement:** The sliding process was conducted by a linear motor (TSMV120-1S). The rotary process was operated by a rotational motor (80BL165S75-3130TK0). The short-circuit current, open-circuit voltage, and transferred charges of the AC/DC-TENG were measured by a programmable electrometer (Keithley model 6514). The capacitance of the capacitor and the charging/discharging curves of the self-charging power system were tested by a potentiostat (Logic, VSP-300, France).

## Supporting Information

Supporting Information is available from the Wiley Online Library or from the author.

## Acknowledgements

L.Z., D.L., and S.L. contributed equally to this work. Research was supported by the National Key R&D Project from Minister of Science and Technology (2016YFA0202704), National Natural Science Foundation of China (Grant No. 61774016, 21773009, 51432005, 5151101243, 51561145021), China Postdoctoral Science Foundation (2019M660587), and Beijing Municipal Science & Technology Commission (Z171100000317001, Z171100002017017, Y3993113DF).

## Conflict of Interest

The authors declare no conflict of interest.

## Keywords

electrostatic breakdown, electrostatic induction, triboelectric charge, triboelectric nanogenerators, triboelectrification

Received: March 14, 2020

Revised: April 10, 2020

Published online:

- [1] Z. L. Wang, *Nano Energy* **2019**, *58*, 669.
- [2] S. Chu, A. Majumdar, *Nature* **2012**, *488*, 294.
- [3] E. J. Markvicka, M. D. Bartlett, X. Huang, C. Majidi, *Nat. Mater.* **2018**, *17*, 618.
- [4] Z. Wen, M. H. Yeh, H. Guo, J. Wang, Y. Zi, W. Xu, J. Deng, L. Zhu, X. Wang, C. Hu, L. Zhu, X. Sun, Z. L. Wang, *Sci. Adv.* **2016**, *2*, e1600097.
- [5] F. R. Fan, Z. Q. Tian, Z. L. Wang, *Nano Energy* **2012**, *1*, 328.
- [6] C. Wu., A. C. Wang, W. Ding, H. Guo, Z. L. Wang, *Adv. Energy Mater.* **2019**, *9*, 1802906.
- [7] Z. L. Wang, J. Chen, L. Lin, *Energy Environ. Sci.* **2015**, *8*, 2250.
- [8] G. Zhu, B. Peng, J. Chen, Q. Jing, Z. L. Wang, *Nano Energy* **2015**, *14*, 126.
- [9] J. Nie, Z. Wang, Z. Ren, S. Li, X. Chen, Z. L. Wang, *Nat. Commun.* **2019**, *10*, 2264.
- [10] S. Niu, X. Wang, F. Yi, Y. S. Zhou, Z. L. Wang, *Nat. Commun.* **2015**, *6*, 8975.
- [11] S. Wang, L. Lin, Z. L. Wang, *Nano Energy* **2015**, *11*, 436.
- [12] J. Wang, Z. Wen, Y. Zi, P. Zhou, J. Lin, H. Guo, Y. Xu, Z. L. Wang, *Adv. Funct. Mater.* **2016**, *26*, 1070.
- [13] Q. Zheng, Y. Zou, Y. Zhang, Z. Liu, B. Shi, X. Wang, Y. Jin., H. Ouyang, Z. Li, Z. L. Wang, *Sci. Adv.* **2016**, *2*, e1501478.
- [14] R. Hinchet, H. J. Yoon, H. Ryu, M. K. Kim, E. K. Choi, D. S. Kim, S. W. Kim, *Science* **2019**, *365*, 491.
- [15] H. Guo, X. Pu, J. Chen, Y. Meng, M. H. Yeh, G. Liu, Q. Tang, B. Chen, D. Liu, S. Qi, *Sci. Rob.* **2018**, *3*, eaat2516.
- [16] J. Luo, Z. Wang, L. Xu, A. C. Wang, K. Han, T. Jiang, Q. Lai, Y. Bai, W. Tang, F. R. Fan, Z. L. Wang, *Nat. Commun.* **2019**, *10*, 5147.
- [17] Y. Zou, P. C. Tan, B. J. Shi, H. Ouyang, D. J. Jiang, Z. Liu, H. Li, M. Yu, C. Wang, X. C. Qu, L. M. Zhao, Y. B. Fan, Z. L. Wang, Z. Li, *Nat. Commun.* **2019**, *10*, 10.
- [18] S. Li, D. Liu, Z. Zhao, L. Zhou, X. Yin, X. Li, Y. Gao, C. Zhang, Q. Zhang, J. Wang, Z. L. Wang, *ACS Nano* **2020**, *14*, 2475.
- [19] X. Pu, H. Guo, J. Chen, X. Wang, Y. Xi, C. Hu, Z. L. Wang, *Sci. Adv.* **2017**, *3*, e1700694.
- [20] J. Wang, S. Li, F. Yi, Y. Zi, J. Lin, X. Wang, Y. Xu, Z. L. Wang, *Nat. Commun.* **2016**, *7*, 12744.
- [21] H. Zou, Y. Zhang, L. Guo, P. Wang, X. He, G. Dai, H. Zheng, C. Chen, A. C. Wang, C. Xu, Z. L. Wang, *Nat. Commun.* **2019**, *10*, 1427.
- [22] S. Li, Y. Fan, H. Chen, J. Nie, Y. Liang, X. Tao, J. Zhang, X. Chen, E. Fu, Z. L. Wang, *Energy Environ. Sci.* **2020**, *13*, 896.
- [23] J. Wang, C. Wu, Y. Dai, Z. Zhao, A. Wang, T. Zhang, Z. L. Wang, *Nat. Commun.* **2017**, *8*, 88.
- [24] S. Lin, L. Xu, W. Tang, X. Chen, Z. L. Wang, *Nano Energy* **2019**, *65*, 103956.
- [25] R. Wen, J. Guo, A. Yu, J. Zhai, Z. L. Wang, *Adv. Funct. Mater.* **2019**, *29*, 1807655.
- [26] X. Yin, D. Liu, L. Zhou, X. Li, C. Zhang, P. Cheng, H. Guo, W. Song, J. Wang, Z. L. Wang, *ACS Nano* **2019**, *13*, 698.
- [27] X. Li., X. Yin, Z. Zhao, L. Zhou, D. Liu, C. Zhang, C. Zhang, W. Zhang, S. Li, J. Wang, Z. L. Wang, *Adv. Energy Mater.* **2020**, *10*, 903024.
- [28] G. Zhu, J. Chen, T. Zhang, Q. Jing, Z. L. Wang, *Nat. Commun.* **2014**, *5*, 3426.
- [29] W. Liu, Z. Wang, G. Wang, G. Liu, J. Chen, X. Pu, Y. Xi, X. Wang, H. Guo, C. Hu, Z. L. Wang, *Nat. Commun.* **2019**, *10*, 1426.
- [30] L. Cheng, Q. Xu, Y. Zheng, X. Jia, Y. Qin, *Nat. Commun.* **2018**, *9*, 3773.
- [31] J. Fu, X. Xia, G. Xu, X. Li, Y. Zi, *ACS Nano* **2019**, *13*, 13257.
- [32] Z. L. Wang, *Nano Energy* **2020**, *68*, 104272.
- [33] Y. Yang, H. L. Zhang, Z. L. Wang, *Adv. Funct. Mater.* **2014**, *24*, 3745.
- [34] J. Luo, L. Xu, W. Tang, T. Jiang, F. R. Fan, Y. Pang, L. Chen, Y. Zhang, Z. L. Wang, *Adv. Energy Mater.* **2018**, *8*, 1800889.
- [35] D. Liu, X. Yin, H. Guo, L. Zhou, X. Li, C. Zhang, J. Wang, Z. L. Wang, *Sci. Adv.* **2019**, *5*, eaav6437.
- [36] C. Zhang, T. Zhou, W. Tang, C. Han, L. Zhang, Z. L. Wang, *Adv. Energy Mater.* **2014**, *4*, 1301798.
- [37] H. Ryu, J. H. Lee, U. Khan, S. S. Kwak, R. Hinchet, S. W. Kim, *Energy Environ. Sci.* **2018**, *11*, 2057.
- [38] S. Wang, L. Lin, Y. Xie, Q. Jing, S. Niu, Z. L. Wang, *Nano Lett.* **2013**, *13*, 2226.
- [39] G. Zhu, J. Chen, Y. Liu, P. Bai, Y. S. Zhou, Q. Jing, C. Pan, Z. L. Wang, *Nano Lett.* **2013**, *13*, 2282.
- [40] C. Zhang, L. Zhou, P. Cheng, X. Yin, D. Liu, X. Li, H. Guo, Z. L. Wang, J. Wang, *Appl. Mater. Today* **2020**, *18*, 100496.
- [41] S. Wang, Y. Xie, S. Niu, L. Lin, C. Liu, Y. S. Zhou, Z. L. Wang, *Adv. Mater.* **2014**, *26*, 6720.
- [42] C. Wu, A. C. Wang, W. Ding, H. Guo, Z. L. Wang, *Adv. Energy Mater.* **2019**, *9*, 1802906.